



Environmental light-activated nanozymes for efficient inactivation of harmful algae and associated hemolytic toxin

Huibo Wang^a, Sidi Liu^b, Zhibin Xu^a, Xiaoyu Weng^a, Changrui Liao^a, Jun He^a, Liwei Liu^a, Yiping Wang^a, Junle Qu^a, Hao Li^{a,*}, Jun Song^{a,*}, Jiaqing Guo^{a,*}

^a State Key Laboratory of Radio Frequency Heterogeneous Integration (Shenzhen University), College of Physics and Optoelectronic Engineering, Key Laboratory of Optoelectronic Devices and Systems of Ministry of Education and Guangdong Province, Shenzhen University, Shenzhen 518060, PR China

^b Department of Biomedical Engineering, University of Groningen and University Medical Center Groningen, 9713 AV Groningen, The Netherlands

ARTICLE INFO

Keywords:

Nanozymes
Reactive oxygen species
Harmful algal blooms
Anti-algal activity
Visible light activation

ABSTRACT

Harmful algal blooms (HABs) pose a significant threat to aquatic ecosystems. Conventional anti-algal methods are associated with low anti-algal efficiency, and absence of treatment of toxins released by algae. Therefore, it is essential to establish effective HAB prevention strategies. Artificial nanozymes have a great potential in combating HABs due to their unique catalytic properties. An ultra-small carbon dots nanozyme (VCN) with oxidase-like activity was synthesized in this study. VCN exerts its catalytic effect by catalyzing the production of reactive oxygen species (ROS) from oxygen. VCN was utilized to inactivate hazardous marine algae based on its catalytic properties. It was found that VCN could rapidly remove more than 90% of harmful algae (*Skeletonema costatum* and *Phaeocystis globosa*) in just 4 h under environmental visible light. To the best of our knowledge, the algae removal efficacy is greater than that of previous reports. Additionally, VCN could attenuate the toxicity of toxins released by algae to counteract secondary pollution caused by algal fragmentation, which is important for practical applications in water pollution caused by algae. Collectively, under applicable and mild conditions, the VCN-presented enzyme activity can efficiently reduce HABs caused harmful pollution.

1. Introduction

Harmful algal blooms (HABs) caused by a variety of different types of algae have become a growing global problem in recent years [1]. In addition to endangering aquatic ecosystems, high densities of algae and the toxins produced by algae pose a grave threat to human safety and causes economic issues, such as causing mass fish kills and increasing costs of the purification of drinking water [2]. Currently, the main methods to approach this global problem include salvage, ultrasound, algaecide (sodium hypochlorite, hydrogen peroxide), photocatalysis, and biological removal [2–14]. However, the application of algae removal strategies such as salvage and ultrasound is limited by their higher cost and difficulty in large-scale use [3]. Although photocatalytic algaecides are a promising strategy to combat algae, the metal elements contained in most photocatalytic algaecides inevitably pose a threat to ecosystems [12,15]. Further, mechanical fragmentation tends to result in the release of algal toxins, and the released toxins will cause greater secondary contamination than algal overgrowth [16,17]. Therefore,

there is an urgent need to develop efficient anti-algal techniques to deal with HABs and the pollution they cause.

Nanozymes are a class of nanomaterials that catalyze the conversion of substrates into products and follow enzyme kinetics [18–22]. As a new generation of artificial enzymes, nanozymes have received widespread attention due to their higher stability than natural enzymes and their ease of mass production [23,24]. Up to now, a variety of nanomaterials, such as metal-based compounds, carbon nanotubes, carbon dots, transition metal oxides/peroxides/dihalides, and metal–organic frameworks have exhibited enzyme-like activities [25–29]. Among the many nanozymes, carbon dots nanozyme showed great potential in the biological field due to their low biotoxicity [30–34]. It was found that nanozymes with mimic peroxidase (POD) and oxidase (OXD) activity are capable of converting hydrogen peroxide or oxygen into toxic ROS, respectively [35]. These excess ROS are able to destroy cell membranes, proteins or nucleic acids, killing a wide range of microorganisms, including bacteria and fungi [36,37]. With the rapid development of nanozymes, they are widely used in biosensing, treatment of bacterial

* Corresponding authors.

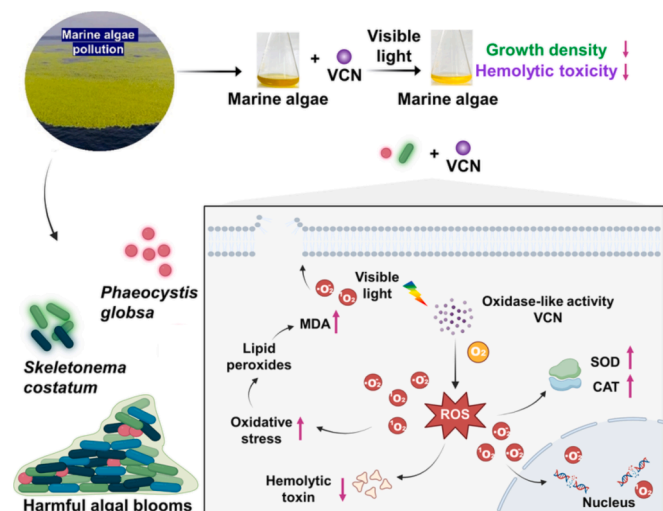
E-mail addresses: lihao000000@163.com (H. Li), songjun@szu.edu.cn (J. Song), 523986726@qq.com (J. Guo).

<https://doi.org/10.1016/j.cej.2023.145029>

Received 12 May 2023; Received in revised form 2 July 2023; Accepted 24 July 2023

Available online 26 July 2023

1385-8947/© 2023 Elsevier B.V. All rights reserved.



Scheme 1. Schematic diagram of the anti-algal activity and inactivation mechanism of VCN against marine harmful algae.

infections, and diagnosis and treatment of cancer [18–23,38]. However, the inactivation of algae by nanozymes is not clear. Therefore, it is challenging to use nanozymes as an anti-algal strategy to combat HABs.

Ideally, anti-algal agents should be able to tolerate salt while inhibiting algal growth and their secreted toxins under mildly environmental conditions. Herein, an ultra-small carbon dots nanozyme was prepared for the inactivation of marine harmful algae. VCN exhibited visible light activated OXD-like activity and the catalytic process of VCN towards the substrate was consistent with the classical kinetic model of enzymatic reactions (Michaelis-Menten equation). According to the Michaelis-Menten equation, the Michaelis constant (K_m) and maximum velocity (V_{max}) of VCN were calculated as 0.29 mM and $1.1 \mu\text{Ms}^{-1}$, respectively. It was reported that most light-activated nanozymes tended to show optimal catalytic activity under acidic or neutral conditions [30,32,39–41], which may make it difficult for them to work in weakly alkaline seawater. In this work, VCN maintained high catalytic activity in buffers with pH values from 4 to 11, in highly concentrated NaCl solution (40 g/L) and at temperatures ranging from 20 to 80 °C, suggesting the prepared VCN could work under harsh conditions. It was found that VCN showed OXD-like activity by catalyzing the generation of ROS from oxygen to oxidize the substrate. Based on the characteristics of VCN, the anti-algal activity and inactivation mechanism of VCN were investigated using two typical marine harmful algae causing red tide, such as *Skeletonema costatum* (*S. costatum*) and *Phaeocystis globosa* (*P. globosa*) as models (Scheme 1). The results indicated that VCN was able to remove more than 90% of harmful algae in a much shorter period of time than other carbon dots without enzyme-like activity [42,43]. Importantly, VCN showed stronger anti-algal activity against harmful algae than observed in previous reports [5,6,11–15,44–51]. Moreover, the hemolytic activity of toxins released by the algae is also inhibited by the VCN, largely reducing the secondary threat posed by the destroyed algae. Next, the anti-algal mechanism of VCN was studied and analyzed by various techniques. VCN was discovered to increase toxic ROS within algal cells when exposed to visible light from the environment. These ROS disrupted the redox balance inside algal cells and induced oxidative stress, leading to destruction of cell wall structure and the death of algal cells. In conclusion, this work has developed a carbon dots nanozyme with oxidase-like activity activated by environmental visible light and elucidated its anti-algal activity and inactivation mechanism against marine harmful algae. This study provides a new strategy for the treatment of HABs and broadens the potential of nanozymes for microbial control application.

2. Materials and methods

2.1. Instruments and reagents

The following reagents were used in the experiments: tartaric acid and diethylaminophenol (Shanghai Aladdin Biochemical Technology Co., Ltd., China), 3, 3', 5, 5'-tetramethylbenzidine (Sigma-Aldrich, USA), F/2 medium (Shanghai Guangyu Biological Technology Co., Ltd., China), sea salt (Shanghai Guangyu Biological Technology Co., Ltd., China), phosphate buffered saline (Biosharp, China), ROS Brite™ 670 (AAT Bioquest Inc., USA), glutaraldehyde (25%, Shanghai Aladdin Biochemical Technology Co., Ltd., China). The kits used were: Cell Counting Kit-8 (Beyotime Biotech Inc., China), superoxide dismutase activity assay kit (Beijing Solarbio Science & Technology Co., Ltd. China), catalase activity assay kit (Beijing Solarbio Science & Technology Co., Ltd., China), and malondialdehyde (MDA) content assay kit (Beijing Solarbio Science & Technology Co., Ltd., China). The following algal species were used: *S. costatum* and *P. globosa* (Shanghai Guangyu Biological Technology Co., Ltd., China). The experimental equipment used included a transmission electron microscope (FEI Tecnai G2 F20, USA), scanning electron microscope (Hitachi SU3500, Japan), Fourier transform infrared spectrometer (Nicolet iS 10, USA), ultraviolet visible absorption spectrometer (Shimadzu UV 1750, Japan), X-ray photoelectron spectrometer (Axis Ultra DLD Kratos AXIS SUPRA, UK), electron spin resonance (ESR) spectroscopy (Bruker EMXplus, Germany), and X-ray photoelectron spectra were fitted using XPS peak41 software. The confocal fluorescence imaging was performed using Laser-scanning confocal fluorescence microscopy (Nikon, A1R MP + and Carl Zeiss, LSM 800 with Airyscan) and Leica SP8 confocal microscopy. The fluorescence intensities of the confocal images were measured using ImageJ software.

2.2. VCN preparation

Tartaric acid (2.3 mmol) and 3-diethylaminophenol (0.9 mmol) were blended in 20 mL of deionized water and then placed in an autoclave lined with polytetrafluoroethylene. The solution mixture was left to react in an oven at a constant temperature of 200 °C. After 48 h, the reaction solution was removed and returned to 20 °C. The reaction solution was filtered and dialyzed via a 0.22 m filter membrane to obtain the VCN solution. The concentration of VCN was assessed by the lyophilization method. 50 mL of VCN solution was frozen at -20 °C for more than 24 h and then lyophilized using a freeze dryer to obtain VCN solids. Finally, the concentration of VCN was calculated from the mass and volume of VCN.

2.3. Oxidase-like activity assessment

2.3.1. Oxidase-like activity assay

The oxidase-like activity of VCN was assessed by colorimetric determination [52]. 3, 3', 5, 5'-tetramethylbenzidine (TMB) is a typical chromogenic substrate for the detection of oxidase activity. In the presence of oxidase, TMB is oxidized and changes from colorless to blue, producing a characteristic peak at 652 nm. The oxidase activity can be assessed based on the degree of oxidation of TMB. The experimental steps were as follows: TMB (40 mM, 100 μL) was mixed with VCN (5 mg/mL, 100 μL) in PBS buffer (800 μL) at 25 °C under environmental visible light irradiation or darkness. Then, the absorbance curves of these mixture were recorded using UV-Vis absorption spectrometer, without TMB as a background.

2.3.2. Determination of catalytic kinetic parameters

The relationship between the rate of VCN-catalyzed substrate oxidation and substrate concentration was analyzed by the classical kinetic model of enzymatic reactions, the Michaelis Menten equation (Eq. (1)) [30]. The maximum reaction velocity (V_{max}) and the Michaelis

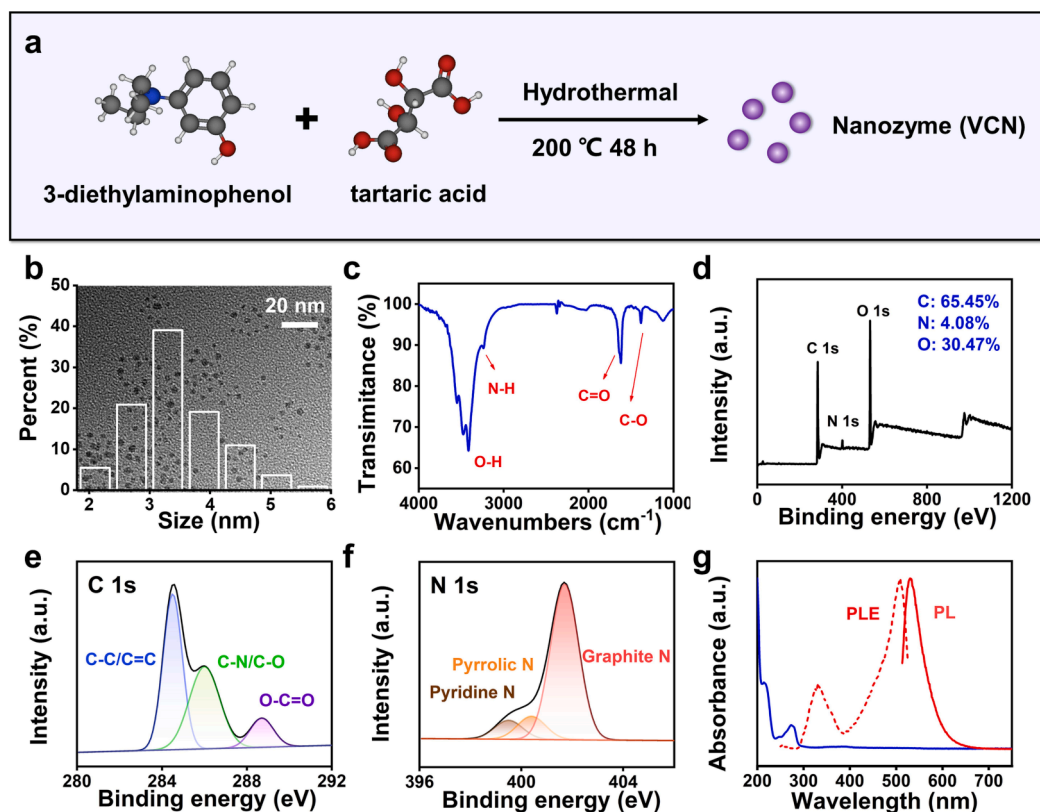


Fig. 1. Characterization of VCN. (a) Diagram of the synthetic route of VCN. (b) TEM image of VCN and the associated particle size distribution. (c) The FTIR spectrum of VCN. (d, e, f) The XPS full spectrum, C 1 s, N 1 s spectra of VCN. (g) The UV-Vis spectrum, PLE and PL spectra of VCN.

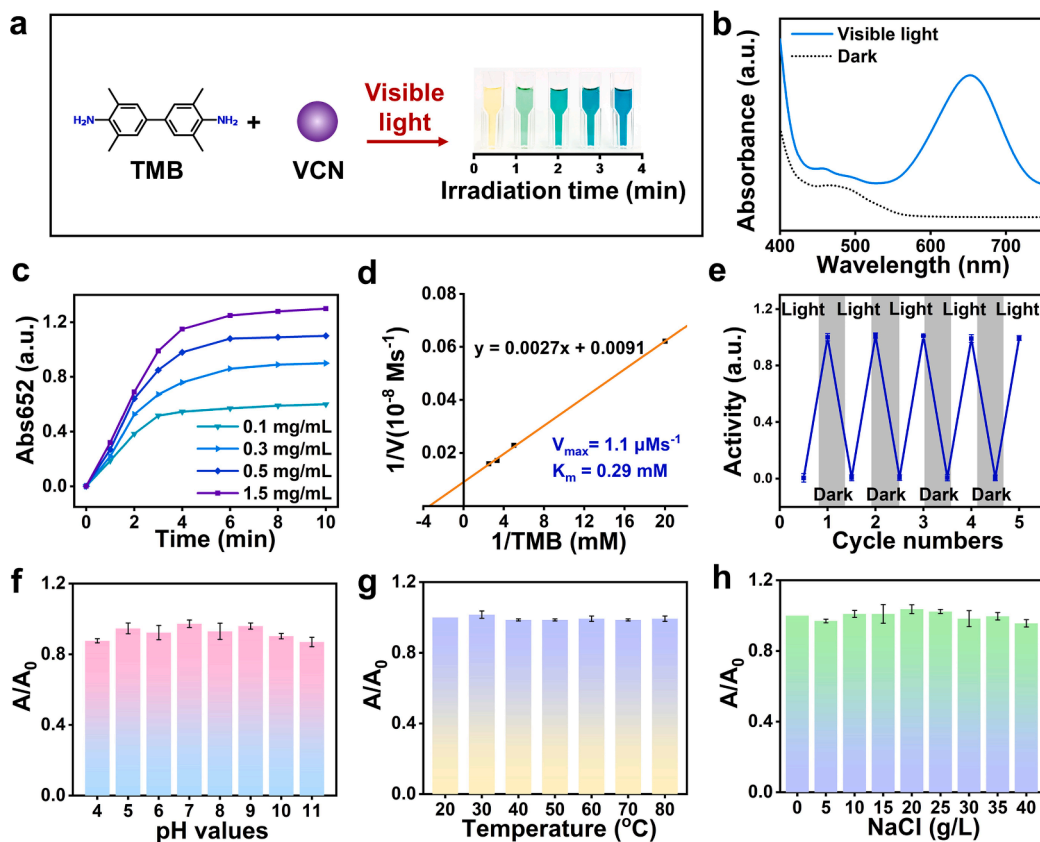


Fig. 2. Oxidase-like activity of VCN. (a) Schematic diagram of VCN-catalyzed substrate oxidation. (b) UV-Vis absorption spectra of the system of VCN and TMB under visible light (blue line) and darkness (black line). (c) Absorbance at 652 nm versus time for the product of catalytic oxidation of TMB by VCN under visible light. (d) Linear fit of the reciprocal of the V_{max} to the reciprocal of the K_m by Lineweaver Burk's double reciprocal plotting. (e) Cycling experiments on the catalytic activity of VCN. (f, g, h) Relative catalytic activity (A/A_0) of VCN in buffer with various pH values (3–12), at different temperatures (20 to 80 °C) and different concentrations of NaCl solutions (0–40 g/L). (For interpretation of the references to color in this figure legend, the reader is referred to the web version of this article.)

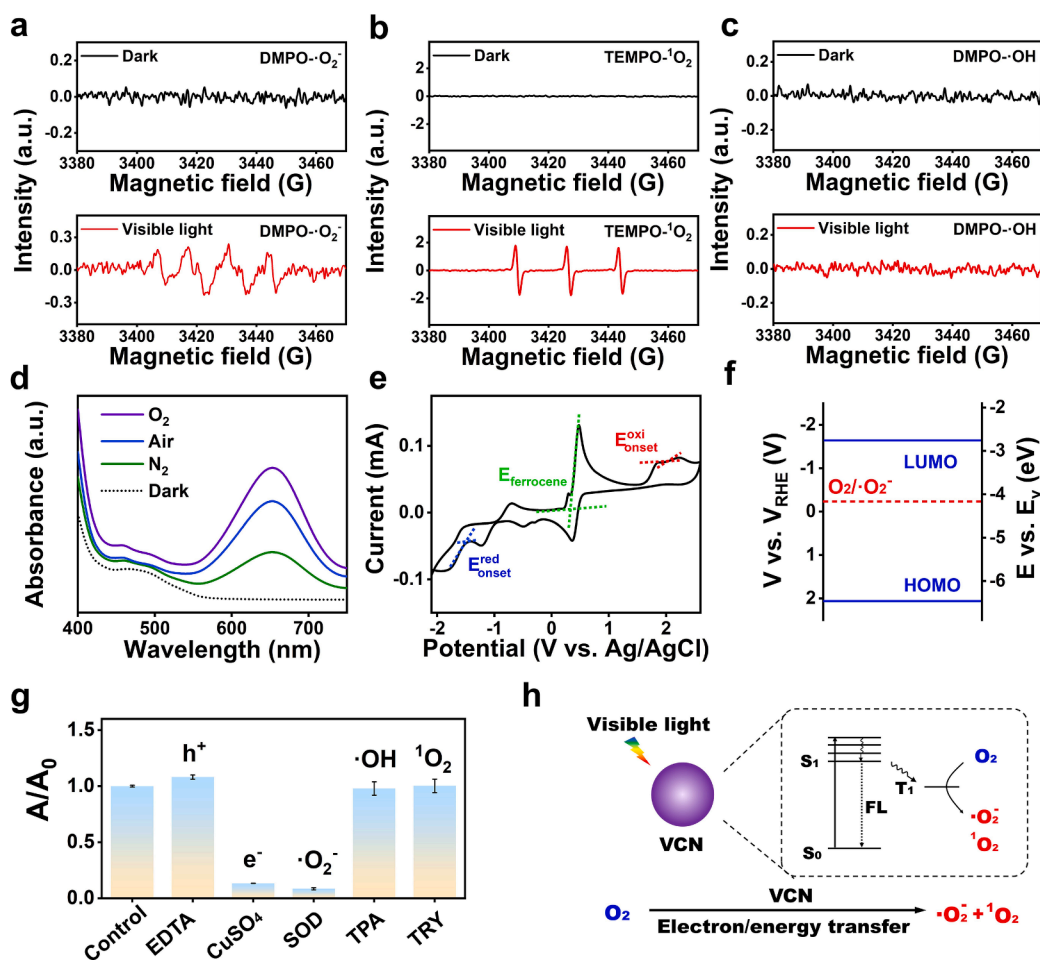


Fig. 3. Catalytic mechanism of VCN as oxidase mimics. (a, b, c) DMPO and TEMPO spin-trapping ESR spectra of VCN under visible light and darkness, respectively. (d) Relative catalytic activity (A/A_0) of VCN in different reaction atmospheres (oxygen, air and nitrogen) under dark/light conditions. (e) Cyclic voltametric curve of VCN with ferrocene as internal standard. (f) The energy band structure diagram of VCN. (g) The effect of different trapping agents, including EDTA, CuSO_4 , superoxide dismutase (SOD), terephthalic acid (TPA), and tryptophan (TRY) on the catalytic activity of VCN. (h) Schematic illustration of the catalytic mechanism of VCN.

constant (K_m) were plotted by Lineweaver Burk's double reciprocal plotting (Eq. (2)). By plotting the linear fit of the reciprocal of the velocity ($1/V$) against the reciprocal of the substrate concentration ($1/[S]$), the V_{max} and K_m values were calculated according to the slope and intercept.

$$V = \frac{[S] \times V_{max}}{[S] + K_m} \quad (1)$$

$$\frac{1}{V} = \frac{K_m}{V_{max}} \times \frac{1}{[S]} + \frac{1}{V_{max}} \quad (2)$$

2.3.3. Stability test

The experiments on the catalytic stability of VCN (0.5 mg/mL) were performed in buffers of different pH values (pH = 4–11), solutions with different concentrations of sodium chloride (0–40 g/L), and solutions with different ions ($25 \mu\text{M}$ of Pb^{2+} , Ag^+ , Zn^{2+} , Mn^{2+} , Ca^{2+} , Fe^{3+} , Mg^{2+} , SO_4^{2-} , HCO_3^- and CO_3^{2-}) and at different temperatures (20–80 °C) [53]. The VCN/TMB mixture without additional ions was set as the control group, and its absorbance value at 652 nm was labeled as A_0 , and the absorbance values measured under the other conditions were labeled as A. The A/A_0 ratio was calculated to evaluate the stability of VCN as an oxidase mimic. Cycling experiments were performed by determining the catalytic activity of the VCN and TMB systems under multiple light–dark cycles by a colorimetric method [54]. Specifically, the system of VCN and TMB was irradiated under visible light condition for 10 min, and the solution changed from colorless to blue. After being left in the dark for 30 min, the color of TMB returned to colorless. Finally, the above steps were repeated to obtain the cyclic experimental data for VCN.

2.4. Anti-algae experiment

The medium required for algal growth was prepared according to the F/2 medium formulation, which included 0.00565 g/L $\text{NaH}_2\text{PO}_4 \cdot \text{H}_2\text{O}$, 0.075 g/L NaNO_3 , 1 mL/L trace metal solution, 1 mL/L vitamin solution and artificial seawater containing 33 g/L sea salt, additionally supplemented in the medium of *S. costatum* with 0.03 g/L $\text{NaSiO}_3 \cdot 9\text{H}_2\text{O}$ [55]. The trace metal solution was obtained by adding to each liter of water with 4.16 g Na_2EDTA , 3.15 g $\text{FeCl}_3 \cdot 6\text{H}_2\text{O}$, 0.01 g $\text{CuSO}_4 \cdot 5\text{H}_2\text{O}$, 0.022 g $\text{ZnSO}_4 \cdot 7\text{H}_2\text{O}$, 0.01 g $\text{CoCl}_2 \cdot 6\text{H}_2\text{O}$, 0.18 g $\text{MnCl}_2 \cdot 4\text{H}_2\text{O}$, 0.006 g $\text{Na}_2\text{MoO}_4 \cdot 2\text{H}_2\text{O}$. The vitamin solution was composed of 0.005 g/L vitamin B12, 0.1 g/L thiamine hydrochloride and 0.0005 g/L biotin. The medium was sterilized by filtration through a 0.22 μm microporous membrane. *S. costatum* and *P. globosa* were seeded into the medium and incubated in an incubator at 25 °C, where the light–dark cycle (LED, 5000 lx) was light: dark = 12 h:12 h [56]. The growth density of the algal cells was determined by measuring the optical density of the algal cells at 680 nm [57]. *S. costatum* and *P. globosa* (10 mL, 2×10^6 cells/L) were treated with different concentrations of VCN (0, 0.35, 0.7, 1.0, 1.5 mg/mL), respectively. The anti-algal performance of VCN was assessed by changes in algal density, and the measurements were corrected using the appropriate concentration of VCN solution as a background in order to avoid the influence of VCN itself on the measurements. The anti-algal rate of algae by VCN was quantified by calculating $(C_0 - C)/C_0 \times 100\%$, where the initial growth density of algae without VCN treatment (control) was denoted as C_0 , and the growth density of algae treated with VCN was denoted as C. In addition, the anti-algal activity of VCN on the marine algae was evaluated. Marine algae collected from Shenzhen Bay were co-mixed with VCN (1.5 mg/ml) and changes in algal density were

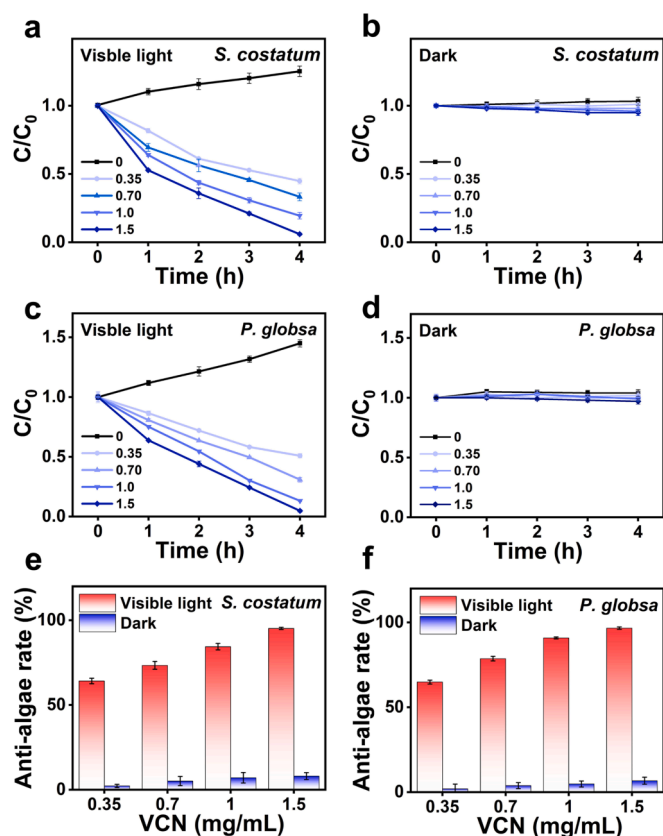


Fig. 4. Anti-algal performance of VCN. (a, b, c, d) Curves of relative growth densities (C/C_0) with time for different concentrations of VCN (0, 0.35, 0.70, 1.0, 1.5 mg/mL) treated with *Skeletonema costatum* and *Phaeocystis globosa* under visible light and darkness, respectively. (e, f) The anti-algae rates of VCN against *Skeletonema costatum* and *Phaeocystis globosa*. Error bars denote standard deviations over three separate parallel experiments.

observed after exposure to visible light for 4 h.

2.5. Analytical methods

2.5.1. Determination of chlorophyll a and chlorophyll b contents

Chlorophyll a (Chl a) and chlorophyll b (Chl b) were extracted using the hot ethanol extraction method [5]. The algal suspension was centrifuged at 8000 rpm for 5 min to obtain the precipitate. After 12 h of freezing at $-20\text{ }^\circ\text{C}$, 2 mL of 95% ethanol ($80\text{ }^\circ\text{C}$) was rapidly added to the precipitate for 2 min, followed by 10 min of sonication. The resulting solution was stored in the dark at $4\text{ }^\circ\text{C}$. After 12 h, the supernatant was obtained by centrifugation at 8000 rpm for 5 min, and the absorbance of the supernatant was measured at 649 (A_{649}), 665 (A_{665}), and 750 (A_{750}) nm. The results obtained were calculated using the modified Lichtenthaler formula, as follows:

$$\text{Chl } a = 13.95 \times (A_{665} - A_{750}) - 6.88 \times (A_{649} - A_{750}) \quad (3)$$

$$\text{Chl } b = 24.96 \times (A_{649} - A_{750}) - 7.32 \times (A_{665} - A_{750}) \quad (4)$$

2.5.2. Extraction of hemolytic toxin

Hemolytic toxin was obtained from *P. globosa* [58]. The extraction procedure was as follows: The algal cell suspension of *P. globosa* was centrifuged at 8000 rpm for 5 min to obtain the algal sediment. The collected algal cells were dispersed into a mixture of chloroform: methanol: water = 13: 7: 5, and then crushed using an ultrasonic cell crusher (600 W, 30 min) at $4\text{ }^\circ\text{C}$. After layering, the lower layer was dried and dissolved in methanol to obtain a crude extract of hemolytic toxin. A mixture of crude extract of hemolytic toxin with different

Table 1

Comparison of the anti-algae activity of different nanomaterials against harmful algae.

Nanomaterials	Algae species	Removal time (h)	Dosage (g/L)	References
TiO ₂	<i>Skeletonema costatum</i>	168	0.03	[6]
Carbon dots	<i>Anabaena</i>	168	0.21	[43]
Cu-MOF-74	<i>Microcystis aeruginosa</i>	120	1	[50]
Co nanoparticles	<i>Skeletonema costatum</i>	96	0.05	[48]
ZnO nanoparticles	<i>Skeletonema costatum</i>	96	0.01	[49]
Nitrogen-doped black TiO ₂	<i>Microcystis aeruginosa</i>	12	0.2	[14]
AP-EGC-CT5	<i>Microcystis aeruginosa</i>	9	2	[13]
PDDA@NPT-EGC	<i>Microcystis aeruginosa</i>	9	2	[44]
Ag ₂ CO ₃ -GO	<i>Microcystis aeruginosa</i>	9	0.1	[11]
MOF-235	<i>Microcystis aeruginosa</i>	6	0.01	[46]
NP-TiO ₂ /C composites	<i>Microcystis aeruginosa</i>	6	4	[45]
Zn-doped Fe ₃ O ₄	<i>Microcystis aeruginosa</i>	6	0.05	[47]
Ag/AgCl@ZIF-8	<i>Microcystis aeruginosa</i>	6	0.01	[12]
Ag ₂ O/gC ₃ N ₄	<i>Microcystis aeruginosa</i>	6	0.05	[5]
Ag ₂ CO ₃ :N: GO	<i>Microcystis aeruginosa</i>	5	4	[15]
PG/Ag ₂ O	<i>Microcystis aeruginosa</i>	5	0.2	[51]
VCN	<i>Skeletonema costatum</i> <i>Phaeocystis globosa</i>	4	1.5	This work

concentrations of VCN (0.35, 0.70, 1.0, 1.5 mg/mL) and then exposed to visible light for 4 h to obtain the crude extract of VCN-treated hemolytic toxin.

2.5.3. Determination of hemolytic activity

The hemolytic activity of hemolytic toxin was tested [58]. 0.5 mL of the crude extract of hemolytic toxin was added to 0.5 mL of isotonic solution of citric acid buffer (3.4 g/L NaCl, 8.6 g/L sodium citrate, 1.8 g/L glucose, pH = 7) and 0.5% (v/v) rabbit red blood cells diluted with isotonic solution of citric acid were added to a water bath at $37\text{ }^\circ\text{C}$ for 30 min. After centrifugation (3000 rpm, 5 min), the absorbance at 540 nm of the supernatant solution was measured, where the fully hemolyzed solution was used as a positive control and the isotonic solution as a negative control. The hemolytic activity was quantified by calculating $(A_s - A_i)/(A_0 - A_i) \times 100\%$, where A_0 , A_i and A_s were the absorbance at 540 nm of the positive control, the negative control and the experimental group, respectively.

2.5.4. Detection of intracellular ROS in algae

The level of ROS in the algal cells was assessed using confocal microscopy [59]. Algae (*S. costatum* and *P. globosa*) treated with VCN (1.5 mg/mL) were incubated in the same environment as the control (without VCN). After 1 h of visible-light irradiation, the obtained algal cells were centrifuged at 8000 rpm for 3 min, washed with PBS three times to remove excess VCN, and then centrifuged at 8000 rpm for another 3 min. The precipitate was then mixed with a ROS detection probe (ROS Brite™ 670) [60]. After incubation for 15–30 min, the algal suspension was obtained by centrifuging (8000 rpm, 3 min) and washing with PBS. The prepared suspension was dropped onto a slide, covered with a coverslip, and fluorescence field images of the ROS Brite™ 670

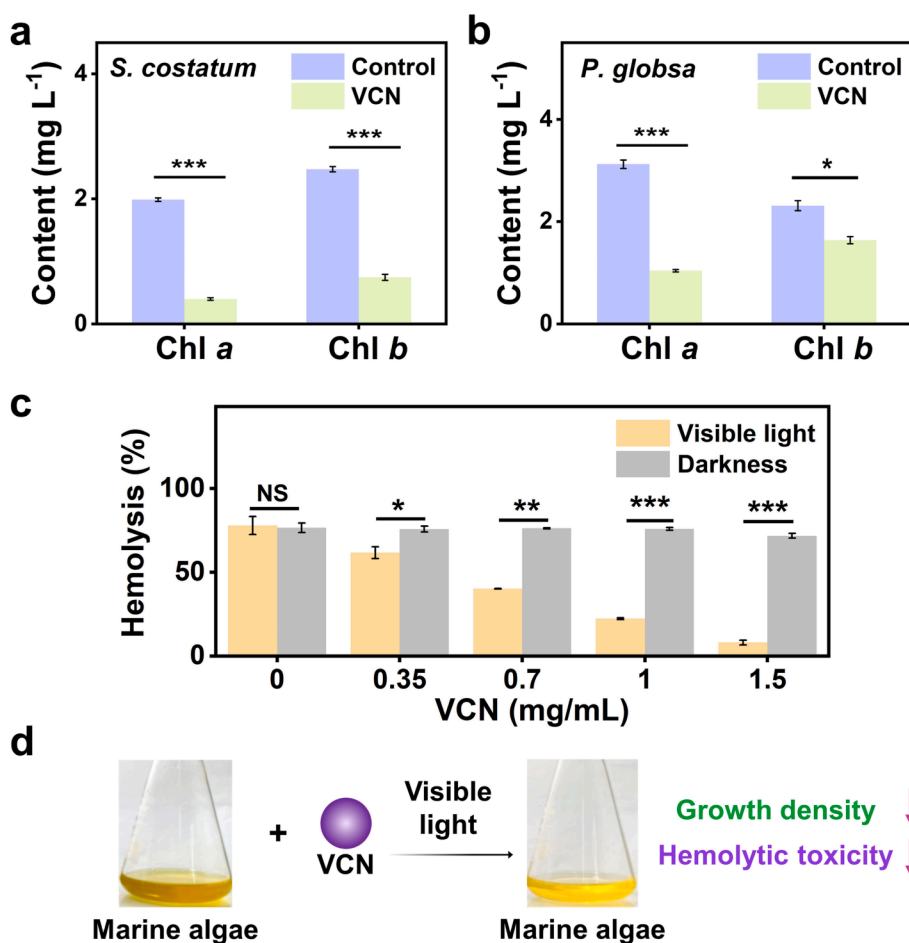


Fig. 5. (a, b) Chlorophyll *a* and Chlorophyll *b* content in untreated (control) and VCN-treated *Skeletonema costatum* and *Phaeocystis globosa*. (c) Hemolytic activity of hemolytic toxin treated with different VCN concentration under visible light and darkness, respectively. (d) Images of the anti-algal effect of VCN on the marine algae. Error bars denote standard deviations from three separate parallel experiments. The significance of the indicated comparisons was calculated using a two-tailed *t*-test, **p* < 0.05, ***p* < 0.01, and ****p* < 0.005. NS indicates no statistically significant difference.

were collected under 647 nm laser irradiation using a confocal microscope.

2.5.5. Determination of SOD activity, CAT activity, and MDA content

Superoxide dismutase (SOD) activity, catalase (CAT) activity, and MDA content of the algal cells were determined and calculated using SOD activity, CAT activity, and MDA content assay kits, respectively. The extraction of SOD, CAT, and MDA from algal cells was performed as follows: the algal cell suspension was centrifuged at 8000 rpm for 5 min to obtain the algal sediment; then, 2 mL of PBS (4 °C) was added, and the solution was incubated at -20 °C for 12 h [51]. The algal cells were repeatedly freeze-thawed three times to break the cells. The supernatant was collected after centrifugation (8000 rpm, 3 min) and used to assess SOD and CAT activity and MDA content.

2.5.6. SEM sample preparation of algae

SEM sample of *S. costatum* and *P. globosa* were prepared by gradient dehydration [48]. *S. costatum* and *P. globosa* incubated with VCN and the control group without VCN were centrifuged at 4000 rpm for 3 min, after which they were soaked in 2.5% glutaraldehyde for 4 h. After centrifugation, the algae were dehydrated over several steps, including soaking and centrifugation at ethanol concentrations of 30, 50, 70, 85, 95, and 100%. The final ethanol solution containing algae was then dropped onto silicon wafers, dried, and examined under a scanning electron microscope.

2.6. Statistical analysis

Data are expressed as mean ± standard deviation (SD). The sample size was five (*n* = 3) unless mentioned otherwise. The significance of the

differences between the groups was calculated using a two-tailed *t*-test. Differences were considered statistically significant at *P* < 0.05. Data were analyzed using Origin v.9.0 (Origin Lab, USA) and Prism software package (Prism 7.0, GraphPad Software, USA).

3. Result and discussion

3.1. Characterization of VCN

The VCN prepared from tartaric acid and 3-diethylaminophenol via hydrothermal method were characterized using a range of techniques (Fig. 1a). TEM image and high-resolution TEM (HRTEM) image of VCN showed that VCN had a near-spherical shape, with a size distribution within 2.1–5.7 nm and 0.21 nm interplanar spacing assigned to the (100) lattice plane of graphite (Fig. 1b and Fig. S1), revealing that VCN have a graphite-like structure. In order to analyze the chemical functional groups of VCN, Fourier transform infrared spectroscopy (FTIR) spectrum of VCN was examined. Many typical peaks were observed in FTIR spectrum of VCN (Fig. 1c), including O-H stretching (broad peaks located at 3546, 3472, 3416 cm⁻¹), N-H stretching (peak located at 3238 cm⁻¹), C = O stretching (peak located at 1618 cm⁻¹), C-O stretching (located at 1386 cm⁻¹), and C-O stretching (located at 1127 cm⁻¹), indicating that VCN had various functional groups such as hydroxyl, amino and carbonyl groups [61]. Furthermore, the elemental composition and structure of VCN were analyzed by X-ray photoelectron spectroscopy (XPS). The full XPS spectrum (Fig. 1d) displayed three characteristic peaks corresponding to C (284.5 eV), N (401.1 eV) and O (531.5 eV) elements and the atomic ratio occupied by each element was 65.45%, 4.08% and 30.47%, respectively. The detailed C, N, and O spectra of the VCN were acquired by split-peak fitting of the data using

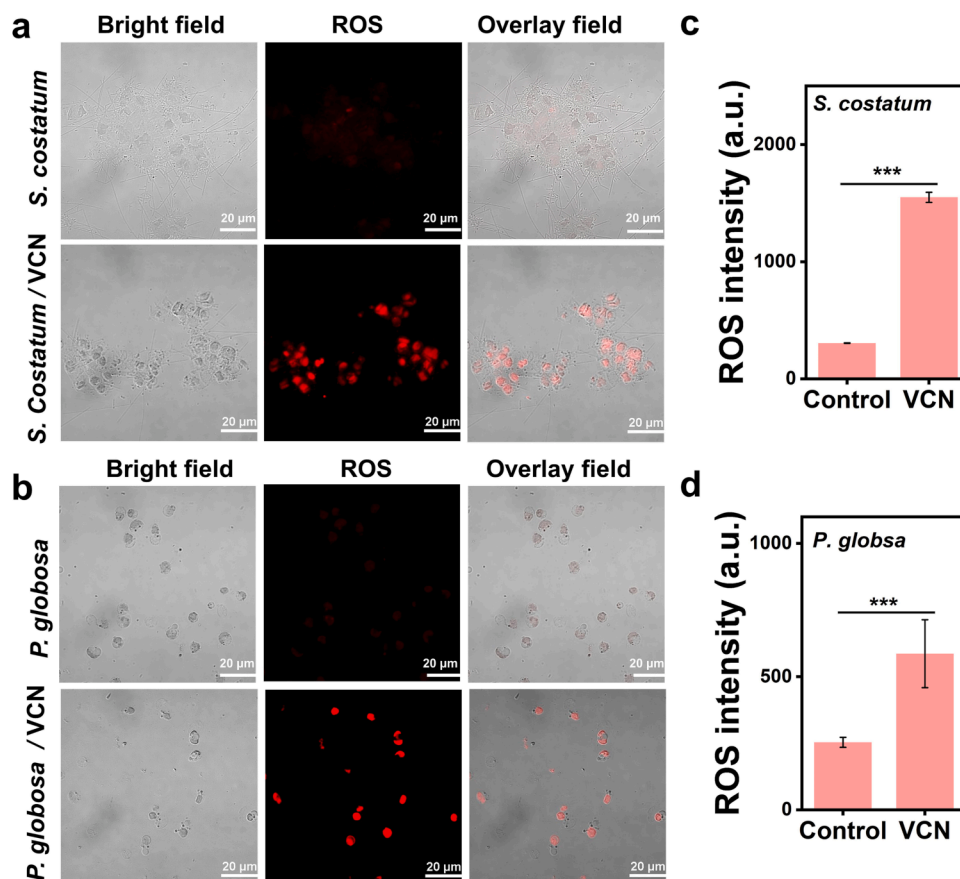


Fig. 6. Anti-algal mechanism of VCN. (a, b) Images of untreated and VCN-treated *Skeletonema costatum* and *Phaeocystis globosa* under bright, fluorescence ($\lambda_{\text{ex}} = 647$, $\lambda_{\text{em}} = 670$ nm), and overlay fields, as measured using confocal microscopy and labeled by ROS detection probes. Scale bar: 20 μm . (c, d) Images of the fluorescence intensities of ROS probes within *Skeletonema costatum* and *Phaeocystis globosa*.

the XPSpeak41 software. The characteristic peaks in the C 1 s spectrum (Fig. 1e) at 284.5, 286.0, and 288.7 eV belong to the C-C/C = C, C-N/C-O and O-C = O bonds, respectively [62]. The N 1 s spectrum (Fig. 1f) clearly shows three distinctive peaks for pyridinic (399.5 eV), pyrrolic (400.4 eV), and graphitic nitrogen (401.7 eV) structures, revealing that VCN was nitrogen-doped [62]. In the O 1 s spectrum, two the typical peaks for the C-O (531.8 eV) and C = O bonds (532.8 eV) could be observed (Fig. S2) [63]. The above results indicated that VCN consists mainly of carbon-based polymers of elemental carbon. The above results suggested that VCN was an oligomer with a predominantly carbon element. Next, the optical properties of VCN were investigated using ultraviolet-visible (UV-Vis) absorption spectrometry and fluorescence spectrometry. As shown in Fig. 1g (blue line), there were two absorption band around in the UV-Vis spectrum of VCN. The strong absorption band around 215 nm is caused by the $\pi-\pi^*$ transition of the C = C bond and the absorption peaks appearing at 275 nm are due to the $n-\pi^*$ transition of functional groups, indicating the formation of carbon core and surface functional groups of VCN [64]. In addition, it was observed in the photoluminescence excitation (PLE) and emission (PL) spectra of VCN (Fig. 1g) that VCN exhibited photoluminescence properties, where the optimal excitation and emission wavelengths were 508 and 530 nm, respectively. To evaluate the biotoxicity of VCN, the cell viability of VCN-incubated 293 T cells at VCN concentrations of (0–3 mg/mL) were determined. The cell viability (Fig. S3) of 293 T cells treated with VCN (0.18, 0.35, 0.70, 1.5, and 3 mg/mL) were 95.0, 92.8, 89.7, 86.5, and 79.6%, respectively. Even after treatment with 3 mg/mL VCN, approximately 80% of the 293 T cells survived, indicating the low cytotoxicity of VCN.

3.2. Visible light activated oxidase-like activity of VCN

To study the oxidase-like activity of VCN, a common oxidase substrate, TMB, was used to assess the catalytic performance of VCN. TMB, as a chromogenic substrate, colorless in itself, will turn blue upon oxidation and produces a distinctive absorption peak at 652 nm. As shown in Fig. 2a, VCN could oxidize the substrate TMB under visible light irradiation, and the blue color of the TMB oxidation product deepens as the irradiation time increases, indicating that VCN has the ability to catalyze the oxidation of TMB. In order to investigate whether the catalytic properties of VCN were triggered by visible light, the UV-Vis absorption spectra of VCN catalyzing the oxidation of TMB under visible light irradiation and dark conditions were measured respectively. It was found that VCN did not oxidize TMB under dark conditions, whereas VCN could oxidize the TMB under visible light irradiation and generated a new absorption peak at 652 nm (Fig. 2b), revealing the oxidase-like activity of VCN could be driven by visible light. In addition, the catalytic oxidation curves of TMB with different concentrations of VCN (0.1, 0.3, 0.5, 1.5 mg/mL) over time showed that VCN had a concentration-dependent and time-dependent oxidase-like activity (Fig. 2c). To better understand the catalytic kinetic of VCN, the K_m and V_{max} of VCN were obtained using Michaelis-Menten model. From the Lineweaver-Burk double reciprocal plots, the K_m and V_{max} of VCN were calculated to be 0.29 mM and 1.1 μMs^{-1} (Fig. 2d). The V_{max} of VCN was higher than that of previously reports (Table S1), indicating a higher catalytic activity of VCN.

In order to evaluate the catalytic stability of VCN, the catalytic activity of VCN under different conditions was tested. Cycling experiments depicted that VCN still maintained over 99% of its catalytic activity after

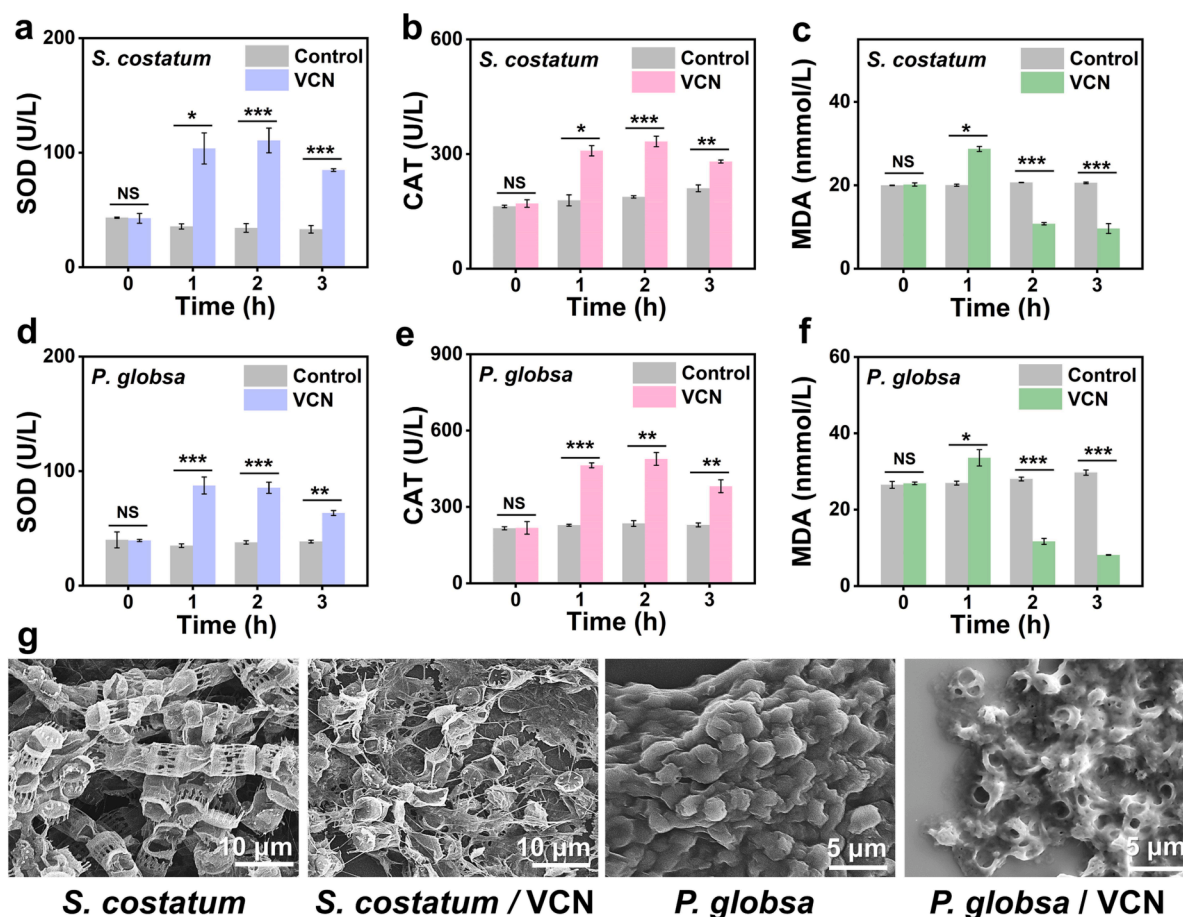


Fig. 7. (a, d) SOD and (b, e) CAT levels and (e, f) MDA content in untreated and VCN-treated *Skeletonema costatum* and *Phaeocystis globosa* at different incubation times. (g) Morphology of VCN-treated *Skeletonema costatum* and *Phaeocystis globosa* was measured using SEM, where untreated VCN were set as controls. Error bars denote standard deviations from three separate parallel experiments. The significance of the indicated comparisons was calculated using a two-tailed *t*-test, **p* < 0.05, ***p* < 0.01, and ****p* < 0.005. NS indicates no statistically significant difference.

five cycles (Fig. 2e). It was reported that most nanozymes have optimal catalytic activity under acidic or neutral conditions (Table S1), while VCN can catalyze at pH values from 4 to 11 (Fig. 2f). Moreover, the catalytic activity of VCN from 20 to 80 °C was independent of temperature, even at 80 °C (Fig. 2g). VCN also kept approximately 97% of its catalytic activity in different concentrations of NaCl solution (Fig. 2h), illustrating that the catalytic activity of VCN was not affected by ionic strength. In addition, the catalytic activity of VCN could reach more than 85% of that of the control in the presence of most ions, such as Pb²⁺, Ag⁺, Zn²⁺, Mn²⁺, Ca²⁺, Fe³⁺, Mg²⁺, SO₄²⁻, HCO₃⁻, and CO₃²⁻ (Fig. S4), indicating that VCN has good catalytic stability. Based on the above observations, VCN displayed the well-tolerated catalytic activity.

3.3. Catalytic mechanism of VCN

In order to explore the catalytic mechanism of VCN, the catalytic behavior and energy band structure of VCN were analyzed using ESR spectroscopy, active species capture experiments and cyclic voltammetry. Based on the fact that the oxidase-like activity of VCN is visible-light driven, the ESR spectra of the possible ROS intermediates produced by VCN under light and dark conditions were detected, respectively. It could be seen that VCN did not generate any ROS under dark conditions (Fig. 3a, 3b, 3c). In contrast, under visible light irradiation, the typical triplet signal (1:1:1) attributed to singlet oxygen (¹O₂) could be detected in the presence of TEMPO as the spin trapping agent. Moreover, the formation of superoxide radicals (⁻O₂[•]) was confirmed using DMPO as the spin-trapping agent. Based on the above observation, VCN was proven to

produce ⁻O₂[•] and ¹O₂ under visible light irradiation. To investigate the origin of these ROS intermediates, the catalytic activity of VCN under different reaction atmospheres (oxygen, air and nitrogen) was tested. The catalytic activity of VCN was higher in atmospheres with high oxygen concentrations than in those with low oxygen concentrations (Fig. 3d), suggesting that VCN may produce ROS intermediates by catalyzing oxygen.

To verify whether VCN had the ability to catalyze the production of ROS from oxygen, the energy band structure diagram of VCN was obtained using cyclic voltammetry. There were multiple oxidation and reduction peaks in the cyclic voltammetric curve of VCN (Fig. 3e). According to the oxidation onset and reduction onset potentials, the positions of the highest occupied molecular orbital (HOMO) and the lowest unoccupied molecular orbital (LUMO) of VCN were calculated, where the energy level of ferrocene was used as a reference. The electron volt in the energy band structure was converted to an electrochemical potential using the reversible hydrogen electrode (RHE) as a standard reference. The energy band structure of VCN (Fig. 3f) displayed that the LUMO potential of VCN was more negative than the energy level from oxygen to superoxide radicals ($E_{O_2/\cdot O_2^-} = -0.23V$), suggesting that VCN could thermodynamically transfer electrons to oxygen and produce superoxide radicals [65].

Furthermore, the effect of several active intermediates trapping agents on the catalytic activity of VCN was examined to discuss which species play the main role in catalyzing the oxidation of TMB. Fig. 3g exhibited that the catalytic activity of VCN was promoted by the capture agent (ethylenediaminetetraacetic acid, EDTA) of holes (h⁺) and

inhibited by the trapping agents (CuSO_4) of electrons (e^-), illustrating that the catalytic process of VCN involved the transfer of electrons. In addition, in the presence of $\cdot\text{O}_2^-$, hydroxyl radicals ($\cdot\text{OH}$), and $^1\text{O}_2$ trapping agents (superoxide dismutase, terephthalic acid, and tryptophan), the catalytic activity of VCN is inhibited only by the superoxide radical trapping agents, implying that $\cdot\text{O}_2^-$ were the main active intermediates in the oxidation of TMB. Overall, VCN could catalyze the formation of $\cdot\text{O}_2^-$ and $^1\text{O}_2$ from oxygen under visible light irradiation by electron or energy transfer (Fig. 3h).

3.4. Anti-algae performance evaluation of VCN

Based on the ability of VCN to catalyze the production of ROS with strong oxidative properties under environmental visible light, the anti-algal activity of VCN against harmful algae in seawater was explored. *S. costatum* and *P. globosa*, as two typical algae causing red tide, were served as model organisms to examine the anti-algal performance of VCN. As shown in Fig. 4a and 4c, both *S. costatum* and *P. globosa* grew normally in the absence of VCN, and the growth of *S. costatum* and *P. globosa* showed different degrees of decrease in the medium containing different VCN concentrations as the incubation time increased under environmental visible light irradiation, demonstrating the algicidal ability of VCN. In contrast, the growth of *S. costatum* and *P. globosa* was not affected by VCN under darkness (Fig. 4b and 4d). In order to more accurately assess the anti-algal activity of VCN, the anti-algal rate of VCN was calculated. It was found that the removal of *S. costatum* and *P. globosa* was greater than 90% after 4 h of treatment of algae with 1.5 mg/mL of VCN under visible light irradiation, whereas under dark conditions, the anti-algal rate of VCN was lower than 10% (Fig. 4e and 4f), indicating that VCN had a visible light-activated anti-algal activity. In addition, the anti-algal rate of VCN increased with increasing VCN concentration under visible light irradiation, revealing that VCN exhibited a concentration-dependent effect on algal inactivation. Moreover, VCN exhibited a shorter removal time against *S. costatum* and *P. globosa* (Table 1), than that reported previously, indicating the higher anti-algal activity of VCN against harm algae [6,43,48–50]. The effect of VCN on algal cell density was also measured by means of hemocytometer plates [66]. As shown in Figs. S5 and S6, VCN could reduce the cell density of *S. costatum* and *P. globosa* under visible light irradiation, which was consistent with the above results. To investigate the anti-algal stability of VCN, the anti-algal activity of VCN at different pH and different concentrations of sea salt solutions were carried out. The anti-algal rates of VCN (1.5 mg/mL) were above 90% at pH from 5 to 11 and sea salt concentrations from 15.0 to 37.5 g/L (Figs. S7 and S8), implying that the pH and salinity used has a negligible impact on the anti-algal performance of VCN. In short, the prepared VCN has visible light-activated algae inactivation.

3.5. Inhibition of algal hemolytic toxin and anti-algal activity in seawater

Based on the above observations, VCN had the ability to kill algal cells and the death of algal cells may result in leakage of the contents of the algal cells, such as chlorophyll and hemolytic substances. Therefore, changes in the content of chlorophyll and changes in the activity of hemolytic toxin for both *S. costatum* and *P. globosa* before and after VCN treatment were measured. It was found that chlorophyll *a* and chlorophyll *b* contents in *S. costatum* and *P. globosa* treated with VCN decreased significantly compared to those before VCN treatment (Fig. 5a and 5b), implicating that VCN could damage algal cells leading to chlorophyll leakage.

The effect of VCN on the hemolytic activity of the toxic substances in the aqueous samples of the algal solution was also assessed, considering that the destructive effect of VCN on the algal cells could also allow the leakage of toxic substances from the algae. Using the sonicated algal solution as a reference, the hemolytic activity of the algal solution treated with VCN (1.5 mg/mL) was reduced (Fig. S9), which may be

attributed to the inactivation of hemolytic toxin by VCN treatment. To verify whether VCN inactivate hemolytic toxin, the influence of VCN on the hemolytic activity of hemolytic toxin extracted from algae was investigated. It was shown that the hemolytic activity (Fig. 5c) of hemolytic toxin treated with different concentrations of VCN under visible light irradiation was 61.6%, 40.1%, 22.3% and 8.07% lower than that of untreated hemolytic toxin (77.9%), implying that VCN could reduce the toxicity of hemolytic toxin.

Based on the efficient anti-algal activity of VCN, the effect of VCN on the treatment of algae collected from seawater was investigated. It was found that VCN treatment reduced the density of marine algae (Fig. 5d) after 4 h of environmental light irradiation, implying that VCN could be used as a highly promising algacide for the removal of marine algae.

3.6. Inactivation mechanism of VCN against algae

Given the ability of VCN to produce ROS *in vitro* and the destructive effects of toxic ROS, it is likely that VCN could inactivate algae by interfering with the redox homeostasis of algal cells. To verify whether VCN kills algae by inducing oxidative stress inside algal cells, the effects of VCN on the ROS levels, antioxidant system and external morphology of algal cells were investigated. First, the levels of ROS in untreated (control) and VCN-treated *S. costatum* and *P. globosa* were detected using a ROS detection probe (ROS Brite™ 670, $\lambda_{\text{ex}} = 647$, $\lambda_{\text{em}} = 670$ nm) to analyze whether VCN increased ROS levels within the algae. It was observed that the fluorescence signal belonging to the ROS Brite™ 670 probe in VCN-treated *S. costatum* and *P. globosa* were significantly increased compared with those in the control (Fig. 6), implying there were large amounts of ROS in VCN-treated *S. costatum* and *P. globosa*. These large amounts of toxic ROS tend to induce oxidative stress in cells. In general conditions, the antioxidant system of algal cells protects them from oxidative stress by scavenging excess ROS. However, when the level of oxidative stress is too high and exceeds the capacity of algal cells to resist it, the antioxidant system of algal cells is disrupted, ultimately leads to algal cell death [5].

In order to identify whether VCN interfered with the antioxidant system of the algal cells, the effect of VCN on the activity of two important enzymes (SOD and CAT) in the antioxidant system of *S. costatum* and *P. globosa* was examined. It was shown that the SOD and CAT levels of VCN-treated *S. costatum* and *P. globosa* were significantly higher than those of the control group after 1 h of exposure to visible light (Fig. 7a, 7b, 7d, 7e), which could be attributed to the activation of the antioxidant enzyme system in algal cells in order to scavenge ROS. The SOD and CAT content in VCN-treated *S. costatum* and *P. globosa* showed a decreasing trend over time, which may be due to a reduction in the number of algal cells as a result of excessive ROS attack. Furthermore, excess ROS can also attack membrane structure of algae, leading to lipid peroxidation. MDA is a biomarker of lipid peroxidation, its level reflects the degree of lipid peroxidation [5]. It was shown that MDA levels in *S. costatum* and *P. globosa* treated with VCN for 1 h were significantly higher than those in the control group (Fig. 7c and 7f), illustrating that VCN caused lipid peroxidation in algal cells. The MDA content in the algal cells treated with VCN for 3 h was significantly lower than that in the control group, which might be due to the rupture of the cell membranes of algal cells after being attacked by ROS.

To study whether VCN disrupts the structure and morphology of algal cells, SEM images of VCN-treated and untreated *S. costatum* and *P. globosa* were acquired. It was found that untreated *S. costatum* and *P. globosa* exhibited normal and complete striped and globular cell morphology, whereas the cell walls of both VCN-treated *S. costatum* and *P. globosa* were disrupted after visible light exposure, and a large number of cell fragments were observed in the field of view (Fig. 7g). The disruption of algal cell morphology by VCN may be a result of VCN-produced ROS attacking the algal cell walls and cell membranes as a protective barrier, eventually leading to cell lysis and cell death. Taken together, the anti-algal mechanism of VCN is as follows: under visible

light irradiation, VCN consumes the oxygen on which algal cells depend while generating large amounts of ROS. Subsequently, these harmful ROS attack the antioxidant system of algal cells and disrupt the oxidative balance, causing the collapse and destruction of cell membranes and cell walls to achieve the removal of algae.

In this study, a visible light activated carbon dots nanozyme was developed for the inactivation of harmful algae. VCN has higher catalytic activity and can inactivate harmful algae more rapidly than previous studies. In addition, VCN not only had anti-algal activity but also reduced the toxic effect of hemolytic toxin from algae. Although this nanozyme exhibited better anti-algal activity against two typical marine harmful algae than previously reported, it still has some drawbacks, such as the difficulty of isolation from seawater. Therefore, future research should focus on the development of degradable nanozymes with anti-algal activity.

4. Conclusion

In conclusion, a metal-free nanozyme (VCN) with visible light-driven oxidase-like activity was constructed for the control of HABs, which catalyzed the production of ROS from oxygen. VCN was used to inactivate hazardous marine algae and was found to remove more than 90% of harmful algae (*Skeletonema costatum* and *Phaeocystis globosa*) in just 4 h under environmental visible light, with greater efficacy than previous reports. VCN could also attenuate the toxicity of toxin released by algae, reducing the impact of secondary pollution caused by algal fragmentation. The study demonstrates that VCN can efficiently reduce harmful pollution caused by harmful algal blooms under mild conditions.

Declaration of Competing Interest

The authors declare no potential conflicts of interest with respect to authorship and/or publication of this article.

CRediT authorship contribution statement

Huibo Wang: Investigation, Writing – original draft, Supervision. **Sidi Liu:** Validation. **Zhibin Xu:** Investigation. **Xiaoyu Weng:** Validation. **Changrui Liao:** Conceptualization. **Jun He:** Software. **Liwei Liu:** Software. **Yiping Wang:** Investigation. **Junle Qu:** Supervision. **Hao Li:** Validation, Supervision. **Jun Song:** Validation, Supervision. **Jiaqing Guo:** Validation, Supervision.

Declaration of Competing Interest

The authors declare that they have no known competing financial interests or personal relationships that could have appeared to influence the work reported in this paper.

Data availability

Data will be made available on request.

Acknowledgements

This work has been partially supported by the National Key R&D Program of China (2021YFF0502900), National Natural Science Foundation of China (62175161 /61835009/62127819), China Postdoctoral Science Foundation (2021M702240). Guangdong Basic and Applied Basic Research Foundation (2023A1515011499/ 2023A1515011114/ 2022A1515111176), Shenzhen Science and Technology Program (JCYJ20210324095810028/JCYJ20210324095613036) and Shenzhen Key Laboratory of Photonics and Biophotonics (ZDSYS20210623092006020). We thank Photonics Research Center of Shenzhen University and Ph.D. Lin for the technical assistance with the Leica SP8 confocal microscopy instrument. Some figures were made by

Biorender.com.

Appendix A. Supplementary data

Supplementary data to this article can be found online at <https://doi.org/10.1016/j.cej.2023.145029>.

References

- [1] A. Trottet, C. George, G. Drillet, F.M. Lauro, Aquaculture in coastal urbanized areas: A comparative review of the challenges posed by Harmful Algal Blooms, *Crit. Rev. Environ. Sci. Technol.* 52 (16) (2022) 2888–2929.
- [2] X. He, P. Wu, S. Wang, A. Wang, C. Wang, P. Ding, Inactivation of harmful algae using photocatalysts: Mechanisms and performance, *J. Clean. Prod.* 289 (2021), 125755.
- [3] B. Balaji-Prasath, Y. Wang, Y.P. Su, D.P. Hamilton, H. Lin, L. Zheng, Y. Zhang, Methods to control harmful algal blooms: a review, *Environ. Chem. Lett.* 20 (5) (2022) 3133–3152.
- [4] L. Hu, R. Wang, M. Wang, Y. Xu, C. Wang, Y. Liu, J. Chen, Research progress of photocatalysis for algae killing and inhibition: a review, *Environ. Sci. Pollut. Res.* 29 (32) (2022) 47902–47914.
- [5] G. Fan, B. Du, J. Zhou, W. Yu, Z. Chen, S. Yang, Stable Ag₂O/g-C₃N₄ p-n heterojunction photocatalysts for efficient inactivation of harmful algae under visible light, *Appl. Catal. B-Environ.* 265 (2020), 118610.
- [6] F. Li, Z. Liang, X. Zheng, W. Zhao, M. Wu, Z. Wang, Toxicity of nano-TiO₂ on algae and the site of reactive oxygen species production, *Aquat. Toxicol.* 158 (2015) 1–13.
- [7] N. Ding, Q. Fei, D. Xiao, H. Zhang, H. Yin, C. Yuan, H. Lv, P. Gao, Y. Zhang, R. Wang, Highly efficient and recyclable Z-scheme heterojunction of Ag₃PO₄/g-C₃N₄ floating foam for photocatalytic inactivation of harmful algae under visible light, *Chemosphere* 317 (2023), 137773.
- [8] Y. Wu, W. Xiang, L. Li, H. Liu, N. Zhong, H. Chang, B.E. Rittmann, A novel photoelectrochemical system to disrupt microalgae for maximizing lipid-extraction efficiency, *Chem. Eng. J.* 420 (2021), 130517.
- [9] D. Wang, J. Chen, X. Gao, Y. Ao, P. Wang, Maximizing the utilization of photo-generated electrons and holes of g-C₃N₄ photocatalyst for harmful algae inactivation, *Chem. Eng. J.* 431 (2022), 134105.
- [10] J. Yang, Q. Zhu, J. Chai, F. Xu, Y. Ding, Q. Zhu, Z. Lu, K.S. Khoo, X. Bian, S. Wang, P.L. Show, Development of environmentally friendly biological algicide and biochemical analysis of inhibitory effect of diatom *Skeletonema costatum*, *Chin. Chem. Lett.* 33 (3) (2022) 1358–1364.
- [11] G. Fan, L. Hong, J. Luo, Y. You, J. Zhang, P. Hua, B. Du, J. Zhan, R. Ning, M. Bao, Photocatalytic inactivation of harmful algae and degradation of cyanotoxins microcystin-LR using GO-based Z-scheme nanocatalysts under visible light, *Chem. Eng. J.* 392 (2020), 123767.
- [12] G. Fan, Y. You, B.o. Wang, S. Wu, Z. Zhang, X. Zheng, M. Bao, J. Zhan, Inactivation of harmful cyanobacteria by Ag/AgCl@ZIF-8 coating under visible light: Efficiency and its mechanisms, *Appl. Catal. B-Environ.* 256 (2019), 117866.
- [13] X. Wang, X. Wang, J. Zhao, J. Song, C. Su, Z. Wang, Adsorption-photocatalysis functional expanded graphite C/C composite for in-situ photocatalytic inactivation of *Microcystis aeruginosa*, *Chem. Eng. J.* 341 (2018) 516–525.
- [14] L.i. Zhou, M. Cai, X.u. Zhang, N. Cui, G. Chen, G.-Y. Zou, In-situ nitrogen-doped black TiO₂ with enhanced visible-light-driven photocatalytic inactivation of *Microcystis aeruginosa* cells: Synthesis, performance and mechanism, *Appl. Catal. B-Environ.* 272 (2020), 119019.
- [15] G. Fan, Z. Chen, L. Hong, B. Du, Z. Yan, J. Zhan, Y. You, R. Ning, H. Xiao, Simultaneous removal of harmful algal cells and toxins by a Ag₂CO₃-N: GO photocatalyst coating under visible light, *Sci. Total Environ.* 741 (2020), 140341.
- [16] L.M. Grattan, V.L. Trainer, Special Issue: Harmful Algal Blooms and Public Health Preface, *Harmful Algae* 57 (2016) 1–1.
- [17] F.M. Van Dolah, D. Roelke, R.M. Greene, Health and ecological impacts of harmful algal blooms: Risk assessment needs, *Hum. Ecol. Risk Assess.* 7 (5) (2001) 1329–1345.
- [18] Y. Zhou, B. Liu, R. Yang, J. Liu, Filling in the gaps between nanozymes and enzymes: Challenges and opportunities, *Bioconjugate Chem.* 28 (12) (2017) 2903–2909.
- [19] D. Jiang, D. Ni, Z.T. Rosenkrans, P. Huang, X. Yan, W. Cai, Nanozyme: new horizons for responsive biomedical applications, *Chem. Soc. Rev.* 48 (14) (2019) 3683–3704.
- [20] J. Wu, X. Wang, Q. Wang, Z. Lou, S. Li, Y. Zhu, L. Qin, H. Wei, Nanomaterials with enzyme-like characteristics (nanozymes): next-generation artificial enzymes (II), *Chem. Soc. Rev.* 48 (4) (2019) 1004–1076.
- [21] H. Wei, L. Gao, K. Fan, J. Liu, J. He, X. Qu, S. Dong, E. Wang, X. Yan, Nanozymes: A clear definition with fuzzy edges, *Nano Today* 40 (2021), 101269.
- [22] L. Gao, L. Chen, R. Zhang, X. Yan, Nanozymes: next-generation artificial enzymes, *Sci. Sin. Chim.* 52 (9) (2022) 1649–1663.
- [23] W. Yang, X. Yang, L. Zhu, H. Chu, X. Li, W. Xu, Nanozymes: Activity origin, catalytic mechanism, and biological application, *Coord. Chem. Rev.* 448 (2021), 214170.
- [24] H. Wang, K. Wan, X. Shi, Recent advances in nanozyme research, *Adv. Mater.* 31 (45) (2019), 1805368.
- [25] Y. Huang, J. Ren, X. Qu, Nanozymes: classification, catalytic mechanisms, activity regulation, and applications, *Chem. Rev.* 119 (6) (2019) 4357–4412.

- [26] X. Xiong, Y. Huang, C. Lin, X.Y. Liu, Y. Lin, Recent advances in nanoparticulate biomimetic catalysts for combating bacteria and biofilms, *Nanoscale* 11 (46) (2019) 22206–22215.
- [27] Y. Li, W. Zhu, J. Li, H. Chu, Research progress in nanozyme-based composite materials for fighting against bacteria and biofilms, *Colloids Surf. B Biointerfaces* 198 (2021), 111465.
- [28] Y. Li, W. Ma, J. Sun, M. Lin, Y. Niu, X. Yang, Y. Xu, Electrochemical generation of Fe₃C/N-doped graphitic carbon nanozyme for efficient wound healing in vivo, *Carbon* 159 (2020) 149–160.
- [29] N.S. Vallabani, A. Vinu, S. Singh, A. Karakoti, Tuning the ATP-triggered pro-oxidant activity of iron oxide-based nanozyme towards an efficient antibacterial strategy, *J. Colloid Interface Sci.* 567 (2020) 154–164.
- [30] S. Li, E. Pang, C. Gao, Q. Chang, S. Hu, N. Li, Cerium-mediated photooxidation for tuning pH-dependent oxidase-like activity, *Chem. Eng. J.* 397 (2020), 125471.
- [31] Y. Lv, M. Ma, Y. Huang, Y. Xia, Carbon dot nanozymes: How to be close to natural enzymes, *Chem.-Eur. J.* 25 (4) (2019) 954–960.
- [32] J. Zhang, S. Wu, X. Lu, P. Wu, J. Liu, Manganese as a catalytic mediator for photo-oxidation and breaking the pH limitation of nanozymes, *Nano Lett.* 19 (5) (2019) 3214–3220.
- [33] X. Li, S. Ding, Z. Lyu, P. Tieu, M. Wang, Z. Feng, X. Pan, Y. Zhou, X. Niu, D. Du, W. Zhu, Y. Lin, Single-atomic iron doped carbon dots with both photoluminescence and oxidase-like activity, *Small* 18 (37) (2022), 2203001.
- [34] J. Jin, L. Li, L. Zhang, Z. Luan, S. Xin, K. Song, Progress in the application of carbon dots-based nanozymes, *Front. Chem.* 9 (2021), 748044.
- [35] M. Xu, Y. Hu, Y. Xiao, Y. Zhang, K. Sun, T. Wu, N. Lv, W. Wang, W. Ding, F. Li, B. Qiu, J. Li, Near-infrared-controlled nanoplatfom exploiting photothermal promotion of peroxidase-like and OXD-like activities for potent antibacterial and anti-biofilm therapies, *ACS Appl. Mater. Interfaces* 12 (45) (2020) 50260–50274.
- [36] L. Mei, S. Zhu, Y. Liu, W. Yin, Z. Gu, Y. Zhao, An overview of the use of nanozymes in antibacterial applications, *Chem. Eng. J.* 418 (2021), 129431.
- [37] D. Yang, Z. Chen, Z. Gao, S.K. Tammina, Y. Yang, Nanozymes used for antimicrobials and their applications, *Colloids Surf. B Biointerfaces* 195 (2020), 111252.
- [38] Y. Chong, Q. Liu, C. Ge, Advances in oxidase-mimicking nanozymes: Classification, activity regulation and biomedical applications, *Nano Today* 37 (2021), 101076.
- [39] W. Liang, Y. Lu, N. Li, H. Li, F. Zhu, Microwave-assisted synthesis of magnetic surface molecular imprinted polymer for adsorption and solid phase extraction of 4-nitrophenol in wastewater, *Microchem. J.* 159 (2020), 105316.
- [40] Y. Liu, M. Zhou, W. Cao, X. Wang, Q. Wang, S. Li, H. Wei, Light-responsive metal–organic framework as an oxidase mimic for cellular glutathione detection, *Anal. Chem.* 91 (13) (2019) 8170–8175.
- [41] J. Li, Y. Xiao, S. Cai, C. Huang, S. Guo, Y. Sun, R.-B. Song, Z. Li, Carbon dots as light-responsive oxidase-like nanozyme for colorimetric detection of total antioxidant capacity in fruits, *Food Chem.* 406 (2022), 134749.
- [42] M. Zhang, H. Wang, P. Liu, Y. Song, H. Huang, M. Shao, Y. Liu, H. Li, Z. Kang, Biototoxicity of degradable carbon dots towards microalgae *Chlorella vulgaris*, *Environ. Sci.-Nano* 6 (11) (2019) 3316–3323.
- [43] H. Li, M. Zhang, Y. Song, H. Wang, C. Liu, Y. Fu, H. Huang, Y. Liu, Z. Kang, Multifunctional carbon dot for lifetime thermal sensing, nucleolus imaging and anti-algal activity, *J. Mater. Chem. B* 6 (36) (2018) 5708–5717.
- [44] X. Wang, X. Wang, J. Zhao, J. Song, C. Su, Z. Wang, Surface modified TiO₂ floating photocatalyst with PDDA for efficient adsorption and photocatalytic inactivation of *Microcystis aeruginosa*, *Water Res.* 131 (2018) 320–333.
- [45] X. Wang, J. Song, J. Zhao, Z. Wang, X. Wang, In-situ active formation of carbides coated with NP-TiO₂ nanoparticles for efficient adsorption-photocatalytic inactivation of harmful algae in eutrophic water, *Chemosphere* 228 (2019) 351–359.
- [46] G. Fan, J. Zhou, X. Zheng, J. Luo, L. Hong, F. Qu, Fast photocatalytic inactivation of *Microcystis aeruginosa* by metal-organic frameworks under visible light, *Chemosphere* 239 (2020), 124721.
- [47] J. Qi, H. Lan, R. Liu, H. Liu, J. Qu, Efficient *Microcystis aeruginosa* removal by moderate photocatalysis-enhanced coagulation with magnetic Zn-doped Fe₃O₄ particles, *Water Res.* 171 (2020), 115448.
- [48] X. Chen, C. Zhang, L. Tan, J. Wang, Toxicity of Co nanoparticles on three species of marine microalgae, *Environ. Pollut.* 236 (2018) 454–461.
- [49] C. Zhang, X. Chen, J. Wang, L. Tan, Toxicity of zinc oxide nanoparticles on marine microalgae possessing different shapes and surface structures, *Environ. Eng. Sci.* 35 (8) (2018) 785–790.
- [50] G. Fan, M. Bao, X. Zheng, L. Hong, J. Zhan, Z. Chen, F. Qu, Growth inhibition of harmful cyanobacteria by nanocrystalline Cu-MOF-74: Efficiency and its mechanisms, *J. Hazard. Mater.* 367 (2019) 529–538.
- [51] Y. Chen, Z. Li, J. Wang, X. Ren, H. Feng, M. Zhang, J. Tang, X. Zhou, L. Tang, Efficient photocatalytic inactivation of *Microcystis aeruginosa* by a novel Z-scheme heterojunction tubular photocatalyst under visible light irradiation, *J. Colloid Interface Sci.* 623 (2022) 445–455.
- [52] D. Zhu, M. Zhang, L. Pu, P. Gai, F. Li, Nitrogen-enriched conjugated polymer enabled metal-free carbon nanozymes with efficient oxidase-like activity, *Small* 18 (3) (2022), 2104993.
- [53] H. Wang, M. Zhang, K. Wei, Y. Zhao, H. Nie, Y. Ma, Y. Zhou, H. Huang, Y. Liu, M. Shao, Z. Kang, Pyrrolic nitrogen dominated the carbon dot mimic oxidase activity, *Carbon* 179 (2021) 692–700.
- [54] H. Li, J. Guo, A. Liu, Y. Chen, Y. He, J. Qu, W. Yan, J. Song, Multi-functional carbon dots for visualizing and modulating ROS-induced mitophagy in living cells, *Adv. Funct. Mater.* 33 (17) (2023), 2212141.
- [55] F. Lananan, A. Jusoh, N. Ali, S.S. Lam, A. Endut, Effect of Conway medium and f/2 Medium on the growth of six genera of South China Sea marine microalgae, *Bioresour. Technol.* 141 (2013) 75–82.
- [56] Q. Wan, J. Li, Y. Chen, Comparative growth and cellular responses of toxigenic *Microcystis* exposed to different types of microplastics at various doses, *Environ. Pollut.* 290 (2021), 117950.
- [57] F. Jia, M. Kacira, K.L. Ogden, Multi-Wavelength Based Optical Density Sensor for Autonomous Monitoring of Microalgae, *Sensors* 15 (9) (2015) 22234–22248.
- [58] X.C. Peng, W.D. Yang, J.S. Liu, Z.Y. Peng, S.H. Lü, W.Z. Ding, Characterization of the hemolytic properties of an extract from *Phaeocystis globosa* Scherffel, *J. Integr. Plant Biol.* 47 (2) (2005) 165–171.
- [59] Z.G. Cardon, E.L. Peredo, A.C. Dohnalkova, H.L. Gershon, M. Bezanilla, A model suite of green algae within the Scenedesmeceae for investigating contrasting desiccation tolerance and morphology, *J. Cell Sci.* 131 (7) (2018), 212233.
- [60] N. Gao, J. Jing, H. Zhao, Y. Liu, C. Yang, M. Gao, B. Chen, R. Zhang, X. Zhang, Defective Ag-In-S/ZnS quantum dots: an oxygen-derived free radical scavenger for mitigating macrophage inflammation, *J. Mater. Chem. B* 9 (43) (2021) 8971–8979.
- [61] H. Wang, F. Lu, C. Ma, Y. Ma, M. Zhang, B. Wang, Y. Zhang, Y. Liu, H. Huang, Z. Kang, Carbon dots with positive surface charge from tartaric acid and m-aminophenol for selective killing of Gram-positive bacteria, *J. Mater. Chem. B* 9 (1) (2021) 125–130.
- [62] S. Ratso, I. Kruusenberg, A. Sarapu, P. Rauwel, R. Saar, U. Joost, J. Aruvali, P. Kanninen, T. Kallio, K. Tammeveski, Enhanced oxygen reduction reaction activity of iron-containing nitrogen-doped carbon nanotubes for alkaline direct methanol fuel cell application, *J. Power Sources* 332 (2016) 129–138.
- [63] H. Wang, H. Li, M. Zhang, Y. Song, J. Huang, H. Huang, M. Shao, Y. Liu, Z. Kang, Carbon dots enhance the nitrogen fixation activity of *Azotobacter Chroococcum*, *ACS Appl. Mater. Interfaces* 10 (19) (2018) 16308–16314.
- [64] H. Wang, M. Zhang, Y. Song, H. Li, H. Huang, M. Shao, Y. Liu, Z. Kang, Carbon dots promote the growth and photosynthesis of mung bean sprouts, *Carbon* 136 (2018) 94–102.
- [65] Y. Zhao, Y. Liu, J. Cao, H. Wang, M. Shao, H. Huang, Y. Liu, Z. Kang, Efficient production of H₂O₂ via two-channel pathway over ZIF-8/C₃N₄ composite photocatalyst without any sacrificial agent, *Appl. Catal. B-Environ.* 278 (2020), 119289.
- [66] C. Camacho-Fernandez, D. Hervás, A. Rivas-Sendra, M. Pilar Marin, J.M. Seguí-Simarro, Comparison of six different methods to calculate cell densities, *Plant Methods* 14 (2018) 30.